Seismic evidence for stratification in composition and anisotropic fabric within the thick lithosphere of Kalahari Craton

Forough Sodoudi, Xiaohui Yuan, Rainer Kind, Sergei Lebedev, Joanne M. -C. Adam, Emanuel Kästle, Frederik Tilmann

Geochemistry Geophysics Geosystems G3

Article
Volume 14, Number 12
26 December 2013
doi: 10.1002/2013GC004955
ISSN: 1525-2027

Published by AGU and the Geochemical Society

Seismic evidence for stratification in composition and anisotropic fabric within the thick lithosphere of Kalahari Craton

Forough Sodoudi
Helmholtz Centre Potsdam, GFZ German Research Centre for Geosciences, Telegrafenberg, 14473 Potsdam, Germany

Freie Universität Berlin, Berlin, Germany (foroug@gfz-potsdam.de)

Xiaohui Yuan
Helmholtz Centre Potsdam, GFZ German Research Centre for Geosciences, Telegrafenberg, Potsdam, Germany

Rainer Kind
Helmholtz Centre Potsdam, GFZ German Research Centre for Geosciences, Telegrafenberg, Potsdam, Germany

Freie Universität Berlin, Berlin, Germany

Sergei Lebedev
Geophysics Section, School of Cosmic Physics, Dublin Institute for Advanced Studies, Dublin, Ireland

Joanne M.-C. Adam
Institut de Physique du Globe de Paris, Paris, France

Emanuel Kästle
University of Potsdam, Institute of Earth and Environmental Science, Potsdam-Golm, Germany

Frederik Tilmann
Helmholtz Centre Potsdam, GFZ German Research Centre for Geosciences, Telegrafenberg, Potsdam, Germany

Freie Universität Berlin, Berlin, Germany

[1] Based on joint consideration of S receiver functions and surface-wave anisotropy we present evidence for the existence of a thick and layered lithosphere beneath the Kalahari Craton. Our results show that frozen-in anisotropy and compositional changes can generate sharp Mid-Lithospheric Discontinuities (MLD) at depths of 85 and 150–200 km, respectively. We found that a 50 km thick anisotropic layer, containing 3% S wave anisotropy and with a fast-velocity axis different from that in the layer beneath, can account for the first MLD at about 85 km depth. Significant correlation between the depths of an apparent boundary separating the depleted and metasomatised lithosphere, as inferred from chemical tomography, and those of our second MLD led us to characterize it as a compositional boundary, most likely due to the modification of the cratonic mantle lithosphere by magma infiltration. The deepening of this boundary from 150 to 200 km is spatially correlated with the surficial expression of the Thabazimbi-Murchison Lineament (TML), implying that the TML isolates the lithosphere of the Limpopo terrane from that of the ancient Kaapvaal terrane. The

largest velocity contrast (3.6–4.7%) is observed at a boundary located at depths of 260–280 km beneath the Archean domains and the older Proterozoic belt. This boundary most likely represents the lithosphere-asthenosphere boundary, which shallows to about 200 km beneath the younger Proterozoic belt. Thus, the Kalahari lithosphere may have survived multiple episodes of intense magmatism and collisional rifting during the billions of years of its history, which left their imprint in its internal layering.

Components: 12,206 words, 11 figures, 1 table.

Keywords: lithospheric layering; S receiver functions.

Index Terms: 7203 Body waves: Seismology; 7294 Seismic instruments and networks: Seismology; 7218 Lithosphere: Seismology; 1236 Rheology of the lithosphere and mantle: Geodesy and Gravity; 0540 Image processing: Computational Geophysics; 0545 Modeling: Computational Geophysics; 1952 Modeling: Informatics; 4255 Numerical modeling: Oceanography: General; 4316 Physical modeling: Natural Hazards; 0935 Seismic methods: Exploration Geophysics; 3025 Marine seismics: Marine Geology and Geophysics.

Received 23 July 2013; **Revised** 12 November 2013; **Accepted** 13 November 2013; **Published** 26 December 2013.

Sodoudi, F., X. Yuan, R. Kind, S. Lebedev, J. M.-C. Adam, E. Kästle, and F. Tilmann (2013), Seismic evidence for stratification in composition and anisotropic fabric within the thick lithosphere of Kalahari Craton, *Geochem. Geophys. Geosyst.*, *14*, 5393–5412, doi:10.1002/2013GC004955.

1. Introduction

[2] The boundary between the lithosphere and asthenosphere (LAB), thought to separate the rigid material of the plates from the underlying convecting material, is a fundamental boundary in plate tectonics, but it has proved to be quite elusive, especially beneath the cratons [*Eaton et al*., 2009; *Romanowicz*, 2009; *Fischer et al*., 2010]. It has long been assumed that ancient cratons contain thick lithospheric roots that are rheologically strong with a chemical buoyancy that counteracts the density increase due to their low temperatures [e.g., *Jordan*, 1975; *Grand and Helmberger*, 1984; *Shapiro et al*., 1999]. However, the depth and nature of the bottom of cratonic lithosphere are still disputed [e.g., *Eaton et al*., 2009; *Rychert et al*., 2010; *Darbyshire et al*., 2013]. New insights on these issues promise essential new constraints on processes of formation and evolution of cratonic lithosphere and its internal architecture.

[3] Different proxies have been used to map the lower limit of the cratonic lithosphere in terms of changes observed in petrological, geochemical, thermal, and geophysical characteristics below and above the LAB [e.g., *Artemieva and Mooney*, 2001; *Griffin et al*., 2003b; *Karato*, 2010, 2012]. In addition, various geophysical techniques have imaged the cratonic LAB as the base of the high-velocity lid [e.g., *Grand*, 2002; *Bartzsch et al*., 2011], a change in anisotropic properties [e.g., *Gaherty and Jordan*, 1995; *Sebai et al*., 2006; *Plomerova and Babuska*, 2010], and a significant reduction in electrical resistivity [*Eaton et al*., 2009; *Jones et al*., 2009]. Analysis of heat flow [e.g., *Jaupart et al*., 1998; *Artemieva*, 2009; *Artemieva and Mooney*, 2001], mantle xenoliths [e.g., *Rudnick et al*., 1998; *Griffin et al*., 2003b], and electrical conductivity [e.g., *Hirth et al*., 2000; *Jones et al*., 2010] data revealed that in general, the rigid part of continental roots is at least 200–250 km thick. Moreover, a wide range of seismic phases and processing methods have been utilized to obtain the depth of the LAB and its corresponding isotropic and/or anisotropic velocity gradients. Recently, surface wave tomography imaged the cratonic lithosphere at depths of about 200–250 km [e.g., *Cammarano and Romanowicz*, 2007; *Kustowski et al*., 2008; *Lebedev and van der Hilst*, 2008; *Lebedev et al*., 2009; *Romanowicz*, 2009] and provided well-constrained estimates of absolute velocity in the lithosphere. Furthermore, vertical variations in velocity anisotropy from surface-wave tomography have also been used to find the relation between the LAB and changes in the strength and orientation of both radial and azimuthal anisotropy [e.g., *Gung et al*., 2003; *Gaherty*, 2004; *Lebedev et al*., 2009; *Yuan and Romanowicz*, 2010]. However, surface waves are only sensitive to smooth velocity variations and are not able to resolve vertical velocity gradients or lateral discontinuities with a precision better than ~50 km. The S receiver function (SRF)

technique [*Farra and Vinnik*, 2000], which is based on S-to-P conversions, has proven to be useful for detecting the LAB with a sufficiently high resolution [*Fischer et al*., 2010; *Rychert et al*., 2010; *Kind et al*., 2012]. This technique is frequently used to find discontinuities identified by a significant negative velocity contrast in the upper mantle [e.g., *Sodoudi et al*., 2006a, 2006b; *Heit et al*., 2007; *Kumar et al*., 2007; *Hansen et al*., 2009; *Sodoudi et al*., 2009; *Abt et al*., 2010; *Ford et al*., 2010; *Geissler et al*., 2010; *Rychert et al*., 2010; *Sodoudi et al*., 2011; *Wölbern et al*., 2012; *Kind et al*., 2013].

[4] However, challenges still remain in detecting the S-to-P conversions from the LAB beneath cratons. Some SRF studies observed a deep (>160 km) negative velocity contrast beneath cratons and interpreted it as the LAB. For example, a deep LAB was reported beneath some parts of the Canadian shield [*Miller and Eaton*, 2010], Kalahari Craton [*Kumar et al*., 2007, *Wittlinger and Farra*, 2007], East European Craton [*Geissler et al*., 2010], Australia [*Kumar et al*., 2007], Scandinavia [*Kind et al*., 2013], and Tanzania Craton [*Wölbern et al*., 2012]. In contrast, other SRF studies found no evidence for the presence of negative discontinuities at these depths beneath the North American Craton [*Abt et al*., 2010; *Kumar et al*., 2012], the Kalahari Craton [*Savage and Silver*, 2008; *Hansen et al*., 2009; *Vinnik et al*., 2009], and in Australia [*Ford et al*., 2010]. Instead they revealed a very sharp negative velocity contrast at much shallower depths (60–150 km).

[5] Recently, *Rychert and Shearer* [2009] used P receiver functions to propose the global existence of the LAB at 90–100 km depth beneath continental cratons, which is much shallower than that derived from surface waves and heat flow analysis. "Mid-Lithospheric Discontinuity" (MLD) has also been proposed [e.g., *Abt et al*., 2010; *Fischer et al*., 2010; *Ford et al*., 2010; *Miller and Eaton*, 2010; *Rychert et al*., 2010; *Wölbern et al*., 2012] as a global characteristic of cratonic lithosphere [*Romanowicz*, 2009], in agreement with the 8° discontinuity, which was previously found in the analysis of dense long-range seismic profiles within the continental lithosphere [*Thybo and Perchuc*, 1997; *Thybo*, 2006]. The nature of the MLD, however, was interpreted differently by different authors and has been attributed to the presence of fluids [*Mierdel et al*., 2007; *Karato*, 2010], remnants of subduction interfaces [*Chen*, 2009; *Miller and Eaton*, 2010], accumulated melts [*Thybo*, 2006; *Ford et al*., 2010; *Wölbern et al*., 2012], or changes in anisotropic properties [*Rychert and Shearer*, 2009; *Yuan and Romanowicz*, 2010]. Further characterization of the MLD is needed to provide more insights into the assembly and evolution of cratons.

[6] In this study, we obtain an improved image of the internal layering of the lithosphere beneath the cratons of southern Africa using the SRF method. In addition, a combined SRF and surface-wave anisotropy analysis provides powerful constraints on the anisotropic properties of the lithosphere.

2. South African Craton (Kalahari Craton)

[7] The Kalahari Craton [*Ashwal and Burke*, 1989] consists of the Archean Kaapvaal and Zimbabwe cratons, which are separated by the Limpopo belt and are surrounded by the Proterozoic Namaqua-Natal belt in the south and by the Proterozoic Kheiss belt in the west (Figure 1). The Kheiss belt (~2.0 Ga) is commonly considered as the Mid-Proterozoic passive margin of the Kaapvaal Craton, deformed in Late Proterozoic time [e.g., *Goodwin*, 1996; *Cornell et al*., 1998; *Griffin et al*., 2003a, 2003b], whereas the Namaqua-Natal belt is likely a Proterozoic terrane accreted to the Kalahari Craton at about 1.2 Ga [e.g., *Matthews*, 1981]. The Kaapvaal Craton is thought to be a collage of different Archean terranes with distinct structural trends assembled and stabilized between 2.6 and 3.1 Ga [*de Wit et al*., 1992]. The Limpopo belt is a terrane that was trapped between the Kaapvaal and Zimbabwe cratons during their collision (2.6–2.7 Ga) but differs in deformational style from them. Furthermore, the Limpopo terrane was thrust over the Zimbabwe Craton, while the Kaapvaal Craton was thrust under the Limpopo terrane during the collisional process [*Durrheim et al*., 1992]. The resulting crustal thickening produced the high metamorphic grade rocks exposed in the Limpopo belt today. High-grade metamorphism (2.7 Ga) and the intrusion of voluminous porphyritic granites and granodiorites (ca. 2.6 Ga) [*Goodwin*, 1996; *Frei et al*., 1999; *Griffin et al*., 2003a] marked the final suturing of the Zimbabwe and Kaapvaal cratons and Limpopo belt into the unified Kalahari Craton. The Kalahari Craton has been progressively modified by metasomatism related to subsequent intraplate and craton-margin magmatism, such as the Bushveld (2.05 Ga) and Ventersdrop (2.5–2.7 Ga), and has been subjected to major flood-basalt events, such as the Karoo (183 Ma), due to the breakup of Gondwanaland in

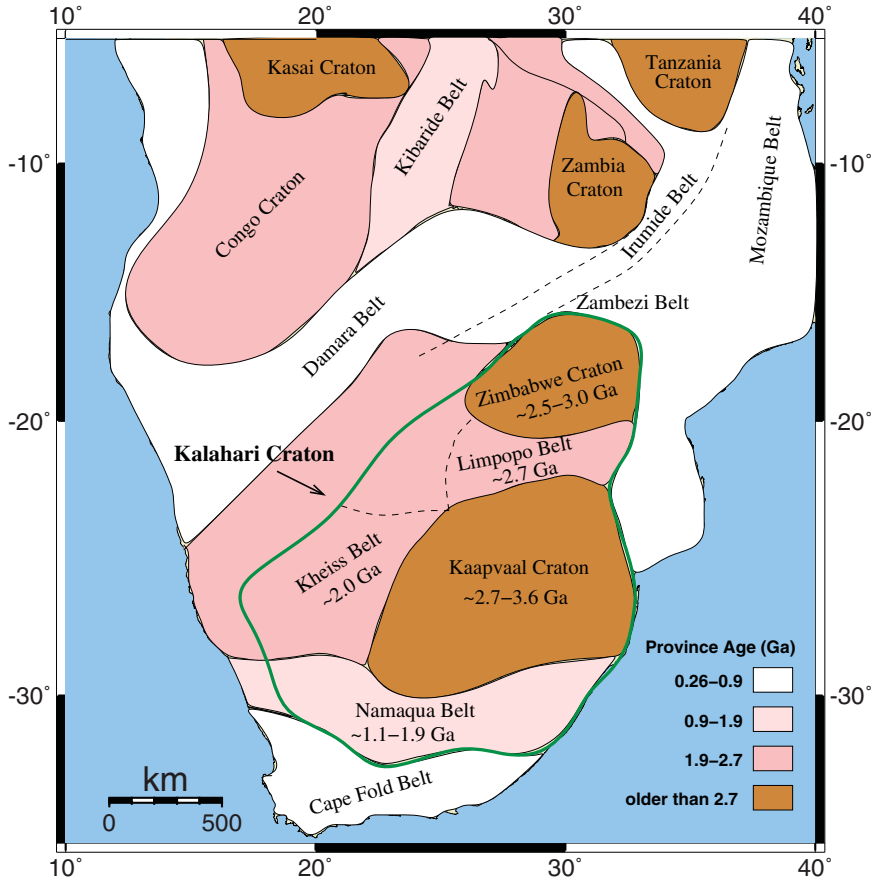

Figure 1. Tectonic map of southern Africa and distribution of Archean and Proterozoic terranes [modified from *Priestley et al*., 2006]. Green line denotes the location of the Kalahari Craton [*Ashwal and Burke*, 1989].

Jurassic time [e.g., *Armstrong et al*., 1987; *Barton et al*., 1994].

[8] A large number of petrological and geochemical studies have been carried out on the mantle nodules from the kimberlite pipes of the Kalahari Craton [e.g., *Gurney and Harte*, 1980; *Boyd and Mertzman*, 1987; *Boyd et al*., 1999; *Griffin et al*., 2003a; *James et al*., 2004]. Additionally, recent geophysical experiments, including the South African Seismological Experiment (SASE) and AfricaArray, have permitted an unprecedented sampling of the seismic structure of the Kalahari Craton. However, the depth extent of the lithosphere varies between studies and often shows little agreement (Table 1). Tomography approaches using body and surface waves have examined the high-velocity lithospheric root beneath the Kalahari Craton. While body wave studies mainly image a thick root extending to depths of 300 km beneath most of the Archean parts of the Kalahari Craton [e.g., *Zhao et al*., 1999; *James et al*., 2001; *Fouch et al*., 2004; *Begg et al*., 2009], a considerably thinner lithosphere (up to 200 km) has been mapped by surface wave studies [e.g., *Li and Burke*, 2006; *Priestley et al*., 2006; *Sebai et al*., 2006; *Chevrot and Zhao*, 2007; *Priestley et al*., 2008; *Fishwick*, 2010; *Adams and Nyblade*, 2011]. Furthermore, no internal layering of the high-velocity root has been detected by either surface wave or body wave tomography. A comparison between the resolutions provided by the two methods [*Priestley and Tilmann*, 2009] clearly reveals good vertical resolution by the regional surface-wave tomography (40–50 km) but poor vertical resolution from the regional body-wave tomography.

[9] Results obtained from SRF analysis show large discrepancies regarding the LAB depth (Table 1). Some authors found a deep discontinuity, down to 300–370 km depth, and interpreted it as the LAB [*Vinnik et al*., 1996; *Kumar et al*., 2007; *Wittlinger and Farra*, 2007]. However, other authors imaged a much shallower boundary at depths of about 140–160 km and interpreted it as either the

Table 1. Previous Studies on the Kalahari Craton and Their Suggested LAB and/or MLD Depth

MLD Depth (km)	LAB Depth (km)	Method	Reference
	160	Body wave tomography	*Zhao et al*. [1999]
	250–300	Body wave tomography	*James et al*. [2001]
	250–300	Body wave tomography	*Fouch et al*. [2004]
	250–300	Body wave tomography	*Begg et al*. [2009]
	150–200	Surface wave tomography	*Priestley et al*. [2006]
	180	Surface wave tomography	*Sebai et al*. [2006]
	180	Surface wave tomography	*Li and Burke* [2006]
	>250	Surface wave tomography	*Chevrot and Zhao* [2007]
	170	Surface wave tomography	*Priestley et al*. [2008]
	200	Surface wave tomography	*Fishwick* [2010]
	150–200	Surface wave tomography	*Adams and Nyblade* [2011]
	370	PRF	*Vinnik et al*. [1996]
	300	SRF	*Kumar et al*. [2007]
160	300	PRF & SRF	*Wittlinger and Farra* [2007]
150		SRF	*Savage and Silver* [2008]
	140	PRF & SRF	*Vinnik et al*. [2009]
	160	SRF	*Hansen et al*. [2009]

LAB [*Hansen et al*., 2009; *Vinnik et al*., 2009] or the MLD [*Savage and Silver*, 2008].

[10] Seismic anisotropy provides important constraints on the ancient assembly of the South African Craton [*Vinnik et al*., 1995; *Silver et al*., 2001, 2004; *Adam and Lebedev*, 2012]. SKS-splitting measurements revealed either anisotropy within the lithosphere due to deformational events in Archean times [*Silver et al*., 2001, 2004] or in the asthenosphere due to deformation in the form of progressive simple shear, which orients the axis of olivine in the direction of plate motion [*Vinnik et al*., 1995]. However, this type of measurement lacks vertical resolution. In contrast, surface-wave anisotropy reveals the distribution of azimuthal anisotropy with depth in southern Africa [*Adam and Lebedev*, 2012]. Based on these findings, anisotropy is present in both the lithosphere and asthenosphere of the Kalahari Craton. In the asthenosphere, fast directions of anisotropy are parallel to the plate motion. In the lithosphere beneath the Limpopo belt and the northern Kaapvaal Craton, fast directions of anisotropy are aligned with the sutures associated with the Archean and Palaeoproterozoic orogenies. Considering all these measurements, a detailed model of mantle anisotropy variations with depth within the Kalahari Craton is still missing.

3. S Receiver Functions

3.1. Data and Analysis

[11] We apply the SRF method to map the internal layering of the lithosphere and to image its lower limit beneath the Kalahari Craton. For this aim, we used teleseismic events recorded at 97 seismic stations within the Archean cratons and Proterozoic mobile belts, including 80 SASE stations [*Carlson et al*., 1996], 14 AfricaArray stations (http://africaarray.psu.edu), and three permanent Global Seismographic Network (GSN, http://www.iris.edu) stations (Figure 2). The SASE stations were deployed between 1997 April and 1999 July, and data from 2006 to 2009 were provided by AfricaArray. Due to the longer recording times of the permanent stations in southern Africa, more than 10 years of data were available for GSN stations. Such a huge amount of data has not been used in any SRF study in South Africa before. We analyzed only S signals from events with high signal-to-noise ratios (larger than 5) occurring at distances of 60°–85° and with magnitudes greater than 5.7 (mb; Figure 3). SRFs are computed by rotating the ZNE component waveforms into the local LQT ray-based coordinate system using the theoretical back azimuth and the selected incident angle, which is found by minimizing the S wave energy and maximizing the amplitudes of the converted signals on the L component [see also *Kumar et al*., 2006; *Sodoudi et al*., 2006b]. Deconvolution of the Q component from the L component provides a source equalization. We reversed the time axis and the polarities of the SRFs and corrected them for moveout using a reference slowness of 6.4 s/deg. To constrain discontinuity depth, SRFs are migrated into the depth domain using the modified IASP91 reference model [*Kennett and Engdahl*, 1991], where the crustal structure was taken from *Hansen et al*. [2009]. An error of at most 5–10 km in the depth estimation of the upper mantle discontinuities may result from uncertainties in the velocity model.

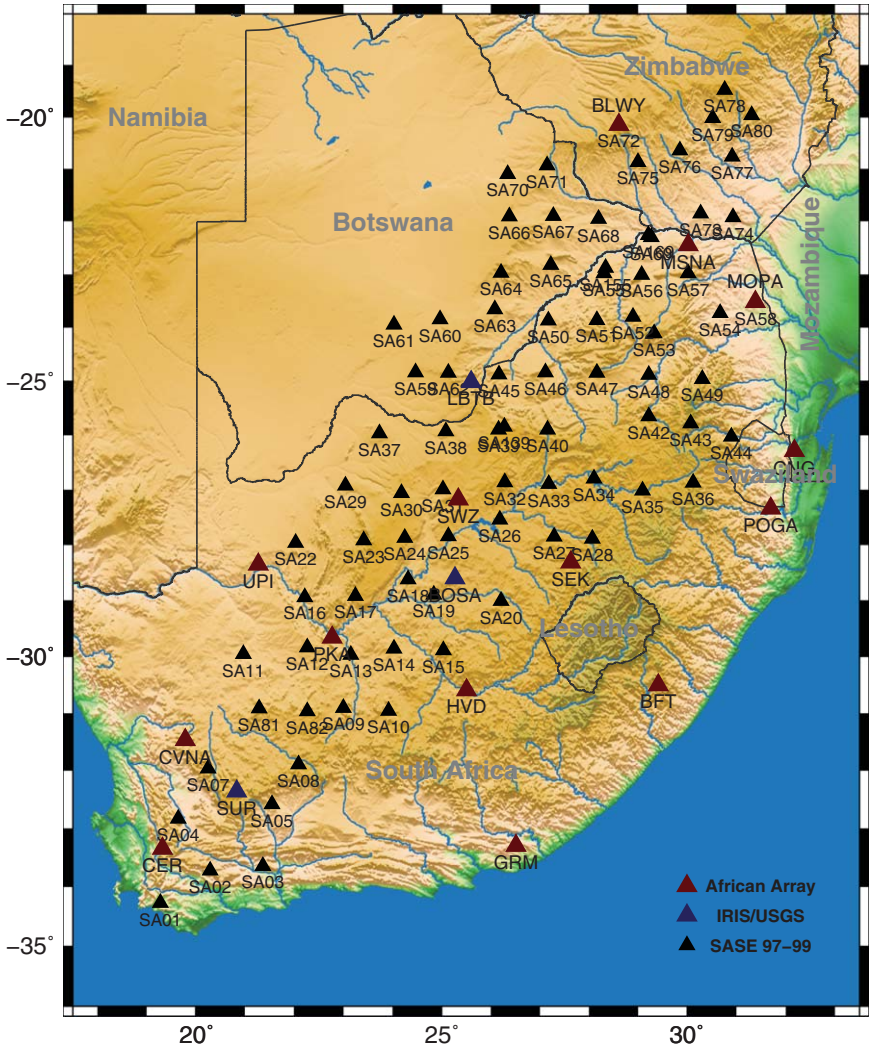

Figure 2. Distribution of 97 seismic stations used in this study.

[12] In total, we obtained more than 500 SRFs from a broad range of azimuths (Figure 3), yielding sufficient azimuthal coverage for anisotropic analysis.

3.2. Observations

[13] S-to-P conversion points at 200 km depth were calculated for all SRF data (Figure 4). This depth is assumed as the approximate depth of the LAB based on previous surface-wave studies (see Table 1). As Figure 4 shows, the Archean cratons and mobile belts are well sampled by the SRFs since the S-to-P conversion points are located about 200 km away from the stations. We projected the 200 km piercing points along a SW-NE trending profile (red line in Figure 4) crossing the whole Kalahari Craton and stacked the corresponding SRFs in bins of 150 km wide in the profile direction (Figure 5). The bin centers are moved in steps of 30 km, resulting in 80% overlap between neighboring stations. A low-pass filter with a 4 s cutoff period was used. The Moho boundary is well imaged at about 4 s as a strong, positive phase indicating an increase in velocity with depth beneath the whole profile. However, we do not focus on the crustal structure of the Kalahari Craton since our aim is to map the LAB and other intralithospheric discontinuities.

[14] In addition to the conversions from the Moho boundary, three pronounced negative phases (decreasing velocity with depth) are evident in the SRF data (shown in gray). The first converted phase, which also shows some S-to-P conversion polarity changes, can be clearly seen at 8–10 s beneath the whole profile (LVZ1). The second negative converted phase (LVZ2) seems to have different delay times beneath different tectonic

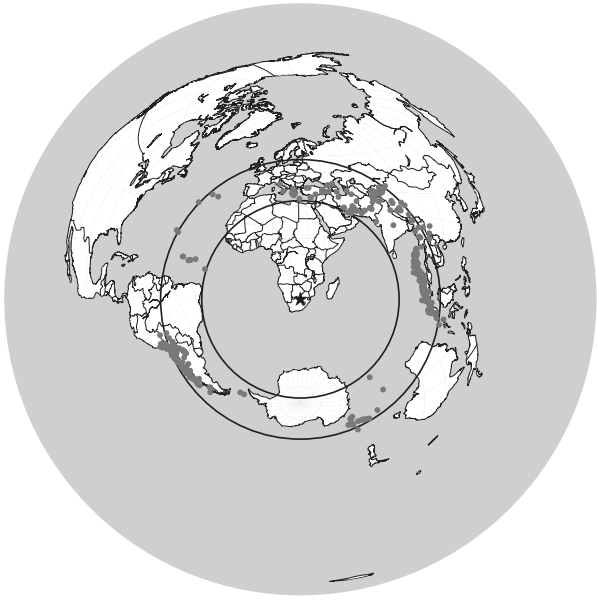

Figure 3. Distribution of teleseismic events utilized to calculate S receiver functions (dark gray dots). The black circles show epicentral distances of 60° and 85°. The black star indicates the approximate location of the network.

terranes. It can be observed at about 15–16 s beneath the northern half of the profile, including the Zimbabwe Craton, the Limpopo belt, and the Mozambique belt, and at about 20–22 s beneath the southern half of the profile, including the Kaapvaal Craton, the Kheiss belt, and the Namaqua-Natal belt. Moreover, the significant jump in delay time (~5 s) along LVZ2 is closely correlated with the surficial expression of the Thabazimbi-Murchison Lineament (TML), which is assumed to be a prominent translithospheric feature with a tectonic history of more than 2.5 Ga [*Good and de Wit*, 1997]. We detect a third negative converted phase at delay times ranging between 27 and 32 s (LVZ3). This phase is clearly imaged beneath the Archean cratons (Zimbabwe, Kaapvaal) and the Limpopo and Kheiss belts.

3.3. Azimuthal Anisotropy From S Receiver Functions

[15] Anisotropy in the upper mantle is thought to reflect the lattice preferred orientation of olivine, which depends on finite shear strain and provides important constraints on the history of deformation of the mantle [e.g., *Silver*, 1996; *Savage*, 1998; *Becker et al*., 2006, *Long and Becker*, 2010]. P receiver functions have occasionally been used as a reliable tool for characterizing seismic anisotropy in the crust and upper mantle [e.g., *Levin and Park*, 1997, 1998; *Bostock*, 1998; *Savage*, 1998; *Frederiksen and Bostock*, 2000] because P receiver functions are dominated by near-receiver shear wave velocity structure and can provide certain constraints on the depth of anisotropy, which cannot easily be inferred from SKS splitting. Splitting of the P-to-S conversions on the receiver functions due to the anisotropy will cause an additional P-to-SH component of motion, which is visible on the transverse component. The characteristic pattern for horizontal anisotropy is the 180° periodicity in the amplitude and polarity of the SH component, and the amplitude variations of the SV component; a good azimuthal distribution is thus required.

[16] S receiver functions are generally not as sensitive to anisotropy as P receiver functions because the S-to-P converted waves do not split in the sense of the shear wave splitting. However, seismic anisotropy does affect the behavior of the SRFs. Azimuthal anisotropy can cause azimuthal variations in the velocity contrast, but variation in anisotropy with depth can also create a new seismic interface, whose velocity contrast is dependent on azimuth. The former effect will cause SRF amplitudes variations, which are usually hard to detect. The latter will create a significant phase with a four-lobed polarity pattern as a function of back azimuth in the SRFs, which can be more easily identified. Below we will show that LVZ1 represents such an anisotropy-induced interface. LVZ2 and LVZ3 are mostly caused by reduction of shear wave velocities.

[17] To characterize the polarity flip observed with the LVZ1 signals (Figure 5), we first check the back azimuthal coverage of each terrane for the largest number of SRFs. As shown in Figure 4, the coverage seems to be sufficient to determine azimuthal anisotropy beneath the Kaapvaal Craton, where we have 454 SRFs. We sort the individual SRFs by their back azimuth and separate them into 90° ranges. To stack the data, SRFs in each range were summed and normalized by the number of events in the range (Figure 6). The uncertainty of the stacked traces is estimated by bootstrapping. We follow the polarity change of S-to-P converted waveforms at ~9 s on the stacked SRFs obtained from different back azimuthal ranges. A significant four-lobed pattern in the polarity of S-to-P conversions with back azimuth is observed among the LVZ1 arrivals.

[18] In order to calculate the synthetic seismograms (SRFs) for the observed four-lobed pattern (Figure 6), we use the ray theory code of

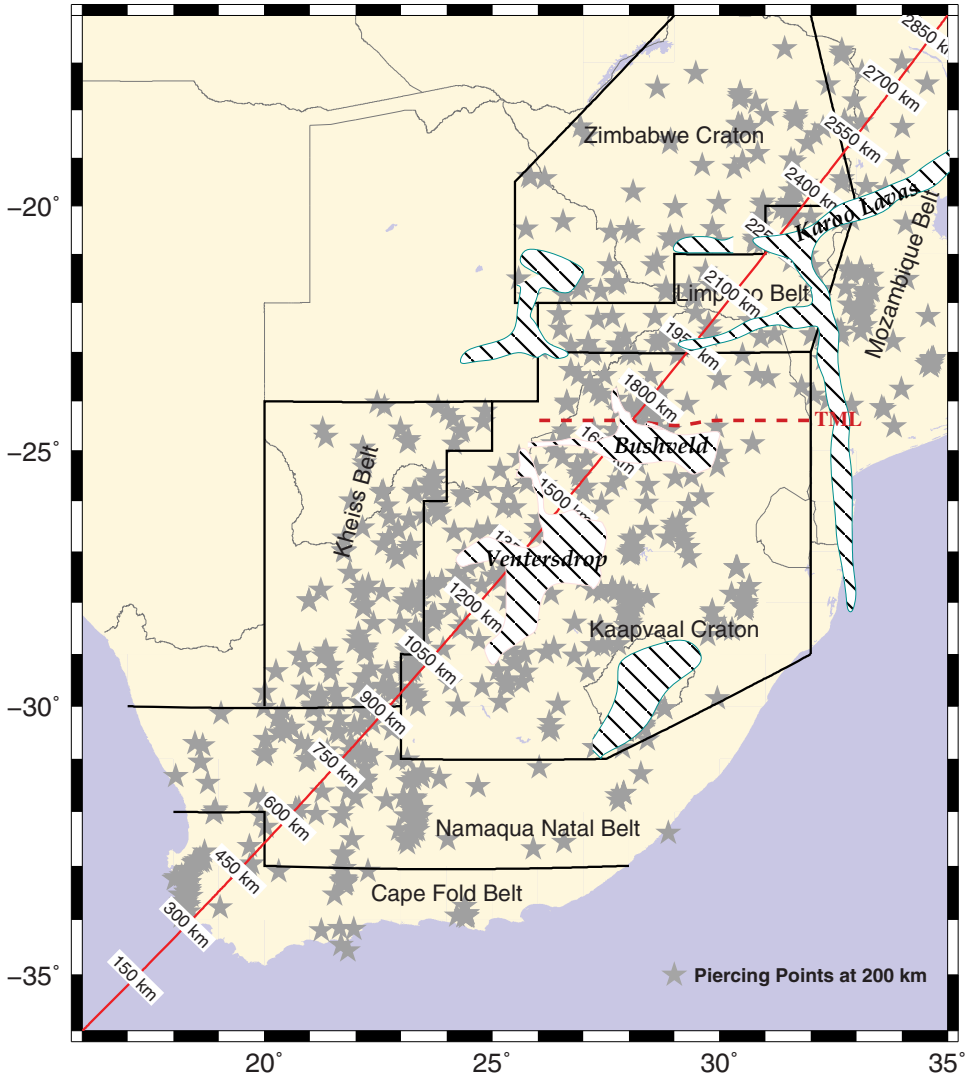

Figure 4. Location of S-to-P piercing points at 200 km depth (gray stars). The boundaries between the Archean cratons and mobile belts are shown with solid black lines. Red solid line marks the position of a SW-NE trending profile used in this study. Green hatched regions represent spatial distribution of the Karoo flood-basalt event (183 Ma); pink hatched areas: Bushveld Complex (2.05 Ga); Ventersdrop (2.5–2.7 Ga). Location of the Thabazimbi-Murchison lineament (TML) is indicated with the red dashed line.

Frederiksen and Bostock [2000] for anisotropic structures. Forward modeling was only performed for the first part of the seismograms (up to 10 s after the direct S arrival), since the other LVZs showed no polarity flip with back azimuth. Using the modified IASP91 reference model, we first converted the arrival times of the converted phases (at ~4.5 and 9 s) to depths. Then, we fixed the Moho depth (at 35 km) and the lower limit of the anisotropic layer (at 85 km), while anisotropy parameters were allowed to vary. Our forward modeling shows that 3% S wave anisotropy and 7% P wave anisotropy with a fast-velocity direction of 45° can match our observations (Figure 7). No significant isotropic velocity contrast is needed to generate the S-to-P conversions observed at ~9 s. As a second step, we fixed the base of the anisotropic layer and the anisotropy parameters and instead change the thickness of the anisotropic layer. Synthetics were calculated and are shown in Figure 7 for thicknesses ranging between 5 and 50 km. The thickness of the anisotropic layer cannot be thinner than 40–50 km as otherwise distinct conversions from the bottom and the top of the anisotropic layer would be observed, contrary to observations. For layer thicknesses of 40–50 km, the conversion from the top merges with the Moho conversion (Figure 6). We were not able to conduct

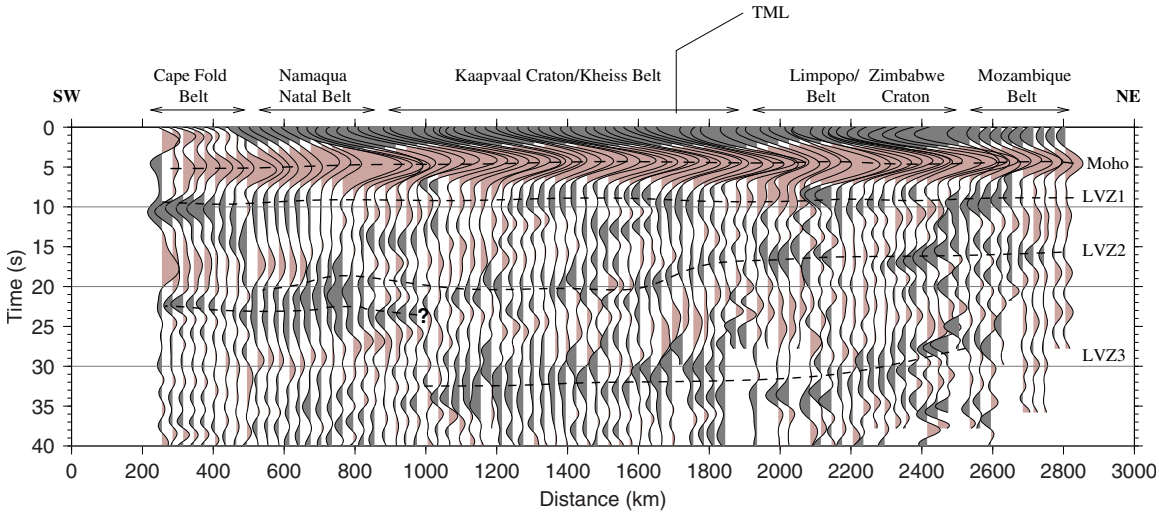

Figure 5. S receiver functions obtained from all stations are projected along the SW-NE trending profile shown in Figure 4 and are stacked in bins of 150 km with a trace interval of 30 km. They are filtered using a low-pass filter of 4 s. Pink (gray) signals show positive (negative) S-to-P converted waves. Besides the converted phase from the Moho, three different negative phases at 8–10 s (LVZ1), 15–22 s (LVZ2), and 27–32 s (LVZ3) are identified beneath the Kalahari Craton. LVZ3 is mostly seen up to the Namaqua-Natal belt, where a much shallower negative phase at 20–22 s is observed (marked with question mark). The TML is located where the LVZ2 seems to suddenly jump from 15 s to 20 s. Note: some S-to-P conversion polarity changes across the LVZ1 are observed along the profile.

the same assessment for other terranes due to non-sufficient data.

3.4. Modeling

[19] SRFs also have the potential to resolve the velocity gradient of a discontinuity. To further constrain the velocity structure, the SRF from the northern half of the region (1700–2800 km along SW-NE profile, see Figure 5) as well as from the southern part of the study area (1000–1700 km along the same profile) were stacked (Figure 8, red lines) and modeled with synthetic receiver functions generated by the ray theory code [*Frederiksen and Bostock*, 2000]. Synthetics were calculated by iteratively fitting the modeled waveform to the observed data utilizing a least squares approach [see also *Wölbern et al*., 2012]. We did not model the first part of the seismograms including the Moho discontinuity and the anisotropic layer, which we have already discussed. Instead, we focused on finding the best fit for delay times larger than 10 s by varying the depth and velocity contrast of each discontinuity in this time range. The model inferred by *Hansen et al*. [2009] for the Kaapvaal Craton was assumed as our starting model. We present our results in Figure 8. Synthetics that best fit the observed, stacked SRFs, and the corresponding optimized models for each section of the study area are separately illustrated. The uncertainty of the stacked traces is estimated by bootstrapping. Relatively abrupt changes in seismic velocities are suggested by our optimal models for both discontinuities. Beneath the northern part of the profile (Figure 8a), our forward modeling indicates that LVZ2 marks a negative velocity contrast at a depth of approximately 152 km. However, this discontinuity is probably at a deeper depth of about 182 km beneath the southern part of the Kalahari Craton (Figure 8b). It is interesting to note that a constant velocity reduction of about 3% was found across LVZ2 beneath the whole Kalahari Craton (except for the Namaqua-Natal belt). Furthermore, LVZ3 indicates a negative velocity contrast at a depth of about 265 km beneath the northern half of the profile. This boundary is also located at a deeper depth of about 282 km beneath the southern half of the profile. Moreover, our optimized model reveals a larger velocity drop of about 4.7% beneath the southern areas, including the Archean Kaapvaal Craton, compared to that of 3.6% found beneath the Limpopo belt and Zimbabwe Craton. To improve the fit to the observed data, which exhibit some additional positive phases between LVZ2 and LVZ3, a gradational velocity increase was also assumed within the lithosphere (between LVZ2 and LVZ3).

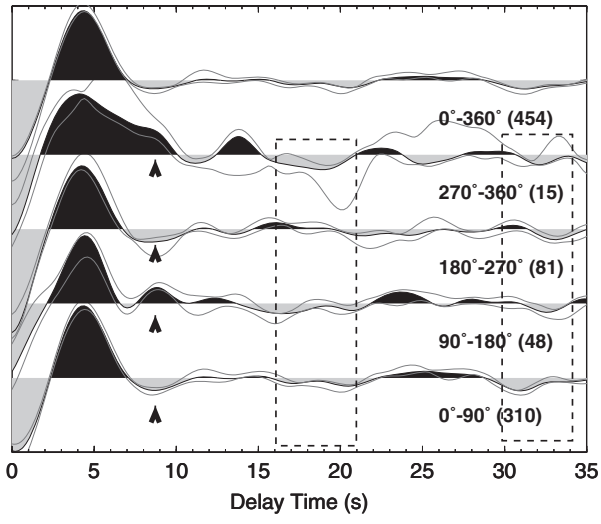

Figure 6. Stacked SRFs obtained from different back azimuth ranges beneath the Kaapvaal Craton. The back azimuth ranges as well as the number of SRFs in each range (in brackets) are shown beneath each stacked SRF. The top trace represents the summation of all SRFs within the Kaapvaal Craton. Gray lines show the 2σ standard deviation intervals obtained from bootstrapping. Black arrows indicate the polarity change of S-to-P converted waves relative to back azimuth at about 9 s (LVZ1). Black dashed boxes mark approximate arrivals of the converted phases from LVZ2 and LVZ3. Note that no polarity change with back azimuth can be seen among LVZ2 and LVZ3.

4. Azimuthal Anisotropy From Surface Waves

[20] Broad-band surface waves are highly sensitive to both the isotropic-average shear speeds and anisotropy in the crust and upper mantle. Anisotropy of surface-wave phase velocities in different parts of southern Africa has been determined recently using thousands of interstation Rayleigh-velocity and Love phase-velocity curves measured in the region [*Adam and Lebedev*, 2012]. The broad period ranges of the measurements (from 5 s to over 200 s) make it possible to constrain the layering of the seismic-velocity structure and anisotropy from the upper crust down to the deep upper mantle.

[21] Inversion of the surface-wave data can yield profiles of the shear-wave speed as well as the azimuthal and radial anisotropy beneath different parts of the Kaapvaal Craton and the Limpopo belt [*Adam*, 2013]. A large positive anomaly in isotropic-average shear speed—characteristic of the cold cratonic lithosphere—is required by surface waves across both tectonic units, down to around 200 km depth, in agreement with published surface-wave tomographic models [e.g., *Priestley and Tilmann*, 2009; *Fishwick*, 2010; *Schaeffer and Lebedev*, 2013].

[22] In Figure 9, we present nonlinear inversions of the phase-velocity data for the azimuthal, shear-wave velocity anisotropy beneath the northern (Figures 9a–9c) and central (Figures 9d–9f) Kaapvaal Craton. Because the result of any single inversion is nonunique, we performed series of inversions, both with smooth (gray bands) and block (blue lines) models [*Agius and Lebedev*, 2013]. Each inversion was a fully nonlinear gradient search, with the synthetic dispersion curve computed directly from a Vs profile at every step using a fast version of the MINEOS modes code (Masters, http://geodynamics.org/cig/software/mineos). The misfits were computed over nine azimuth-specific dispersion curves, with the azimuths spaced uniformly at a 20° intervals. The phase-velocity curve for each azimuth differs from those at other azimuths due to the anisotropy of phase velocities, which we know as a function of period from the measurements of *Adam and Lebedev* [2012]. The cumulative misfits are shown in Figures 9c and 9f; all models shown fit the data approximately equally well.

[23] At around 80–90 km depth, surface-wave data require substantial changes in fast-propagation directions beneath different parts of the Kaapvaal Craton (Figure 9). However, surface-wave data alone cannot resolve whether these changes are sharp or occur over broad depth intervals: the data can be fit equally well by models with sharp and gradual anisotropy variations. Receiver functions, in contrast, resolve a discontinuity in anisotropy but not the average anisotropy in the layers above and below the interface.

[24] The joint analysis of SRFs and surface-wave anisotropy thus yields more information on the lithospheric structure than analysis of any one of the data sets could. By combining SRF and surface-wave data, we can establish that the upper and lower lithospheric mantle layers have distinctly different anisotropy and are separated by a sharp discontinuity at 80–90 km depth.

5. Discussion

[25] We migrated the SRFs to depth and plot them along the SW-NE profile indicated in Figure 4 (Figure 10). A low-pass filter with a 6 s cutoff period is applied in order to better image the

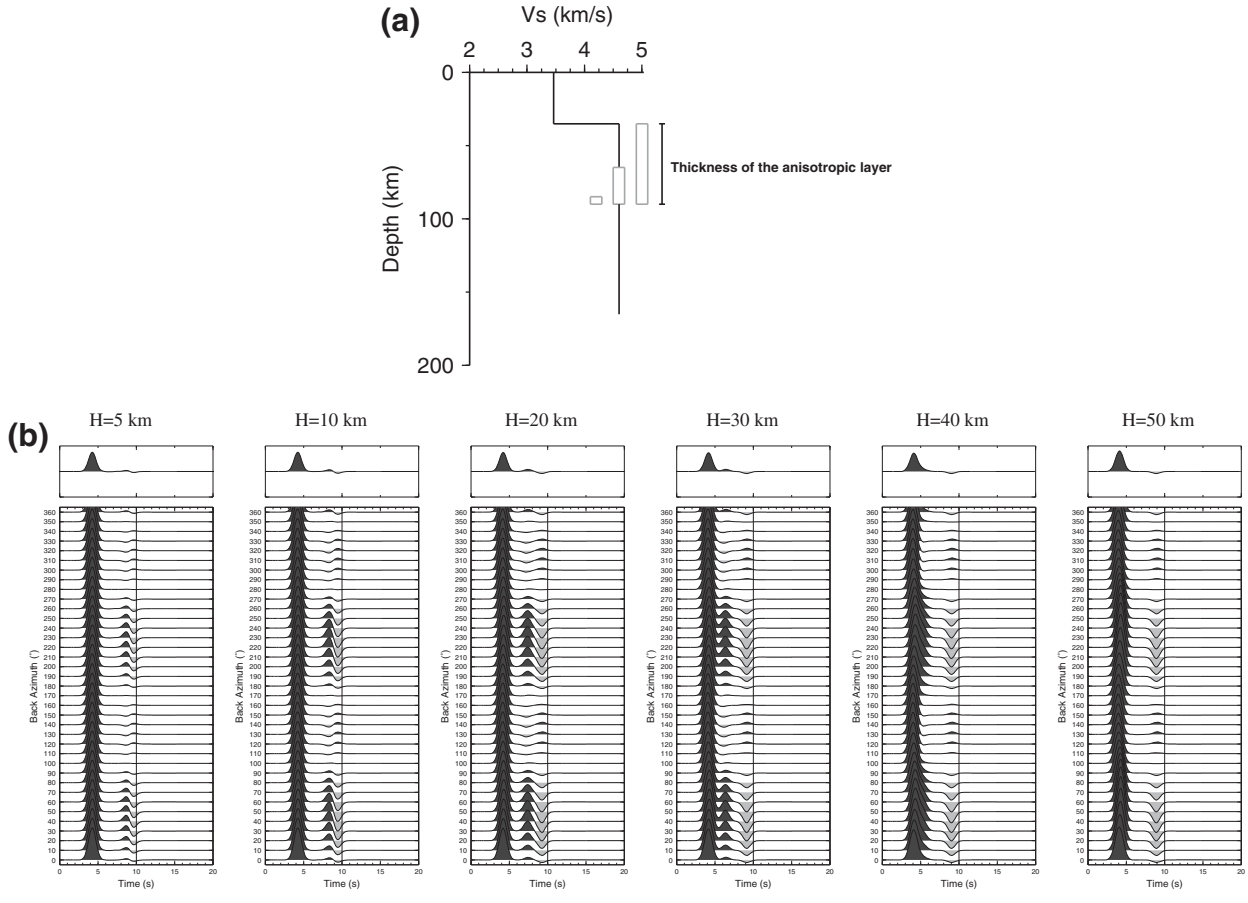

Figure 7. Synthetic SRFs obtained from an anisotropic model containing 3% S wave and 7% P wave anisotropy, with a fast-velocity direction of 45°. This model can reproduce the converted phase at ~9 s showing polarity changes with back azimuth. (a) Anisotropic layer with varying thicknesses (5–50 km) are assumed and modeled. (b) Corresponding synthetic SRFs for different anisotropic layer thicknesses. The top traces represent the stacks of all traces in the lower panels. Results show that a thickness of ~50 km can optimally fit the SRF data.

coherent and continuous signals over a large distance. The migrated SRFs show evidence for an irregularly stratified and thick lithosphere beneath the Kalahari Craton, containing three consecutive negative velocity contrasts: LVZ1 at 85 km, LVZ2 at 150–200 km, and LVZ3 at 260–280 km depth. These depths match those obtained from our modeling. The presence of the 410 km discontinuity further confirms the reliability of our processing. We also observe a positive velocity contrast at depths of about 230–240 km throughout the whole profile, which may be attributed to the Lehmann discontinuity beneath shield areas, as suggested by *Thybo* [2006].

[26] We compare our results with those derived from previous SRF studies (Table 1). Although the processing steps generally used appear to be similar, the selection and filtering of the data may be an important factor affecting the SRFs obtained [*Rychert et al*., 2010]. Most of the earlier studies in the Kalahari Craton resolved either a LVZ at 140–160 km depth [*Savage and Silver*, 2008; *Hansen et al*., 2009; *Vinnik et al*., 2009], matching our LVZ2 beneath the northern half of the profile, or a pronounced velocity reduction at 300 km depth [*Kumar et al*., 2007; *Wittlinger and Farra*, 2007], which is consistent with our LVZ3. No evidence for the presence of LVZ1 has been presented before.

[27] The closest study to our own was conducted by *Wittlinger and Farra* [2007], who imaged two negative discontinuities at 160 and 300 km within the lithosphere of the Kaapvaal and Zimbabwe cratons. However, they did not map the lateral variations of these discontinuities with the same resolution as we have done (Figures 5 and 10). They inferred a lithospheric thickness of about 300 km, with a 160 km thick anisotropic layer beneath the

Moho with a vertical slow axis, overlaying a 100 km thick isotropic layer. Moreover, they roughly estimated the depth of the first discontinuity and located it within a wide depth range from 80 to 160 km. Within this depth range (80–160 km), however, our results clearly show two pronounced LVZs (LVZ1, LVZ2) with distinct characteristics. We clearly identify LVZ1 at 85 km as the bottom of a distinctly anisotropic layer (at least beneath Kaapvaal Craton) with a thickness of 40–50 km. This finding was also confirmed by surface-wave azimuthal anisotropy beneath the Kaapvaal Craton, which shows major changes in the fast-direction orientation around 80–90 km depth.

[28] The depth of the LVZ1 discontinuity fits well with that of *Rychert and Shearer* [2009], who suggested a shallow LAB at about 90–95 km depth beneath Precambrian shields. They also proposed that this discontinuity may be due to a change in seismic anisotropy. Indeed, a thermal LAB so shallow would be difficult to reconcile with evidence from surface waves or xenoliths, and there is abundant evidence for seismic anisotropy within the mantle lithosphere. As we have shown in this paper, both receiver functions and surface waves indicate a change in anisotropy around 80–90 km depth beneath southern Africa that can account for the LVZ1 conversions.

[29] Anisotropic parameters estimated from our SRF modeling beneath the Kaapvaal Craton included a fast-axis direction of 45° in the uppermost mantle. Results inferred from SKS splitting display a coherent spatial pattern for the fast-propagation azimuths, changing from NNE-SSW in the southwestern Kaapvaal to NE-SW further north, and to nearly E-W beneath in the Limpopo belt [*Silver et al.*, 2001, 2004]. Surface-wave anisotropy reveals layered azimuthal anisotropy in the lithosphere and asthenosphere that gives rise to the shear wave splitting [*Adam and Lebedev*, 2012]. In the Limpopo belt and the northernmost Kaapvaal Craton, a very similar pattern of anisotropic layering has been obtained independently in a joint inversion of receiver functions and SKS

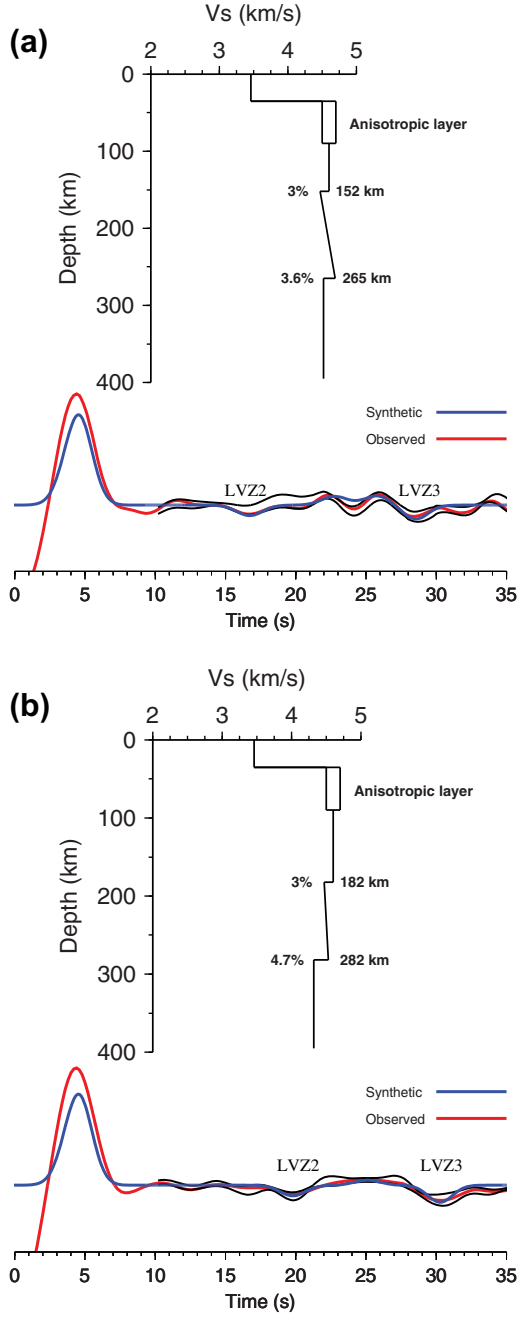

Figure 8. Velocity models for the (a) northern and (b) southern parts of the profile shown in Figure 4. Thick red lines are observed data, and blue lines show the synthetic waveforms. Thin black lines indicate the 2σ standard deviation intervals obtained from bootstrapping (from 10 s). The seismograms are fit for times from 10 to 35 s only. (a) Summation trace obtained from SRFs from the Zimbabwe Craton and the Limpopo belt (red). The synthetic SRF (blue) shows the best fit. The corresponding velocity model (upper) clearly indicates two significant LVZs at 152 km (LVZ2) and 265 km (LVZ3) within the lithosphere. LVZ3 seems to be stronger (velocity drop of 3.6%) than LVZ2 (velocity drop of 3%). (b) Same as Figure 8a but for the Kaapvaal Craton and the Kheiss belt. Both discontinuities are located deeper than those in the northern part of the profile. LVZ3 shows a larger velocity drop beneath the older Kaapvaal Craton and its margin than that beneath the younger Zimbabwe Craton and the Limpopo belt. Increasing velocity between LVZs was added to the model to construct the positive phases observed between LVZ2 and LVZ3.

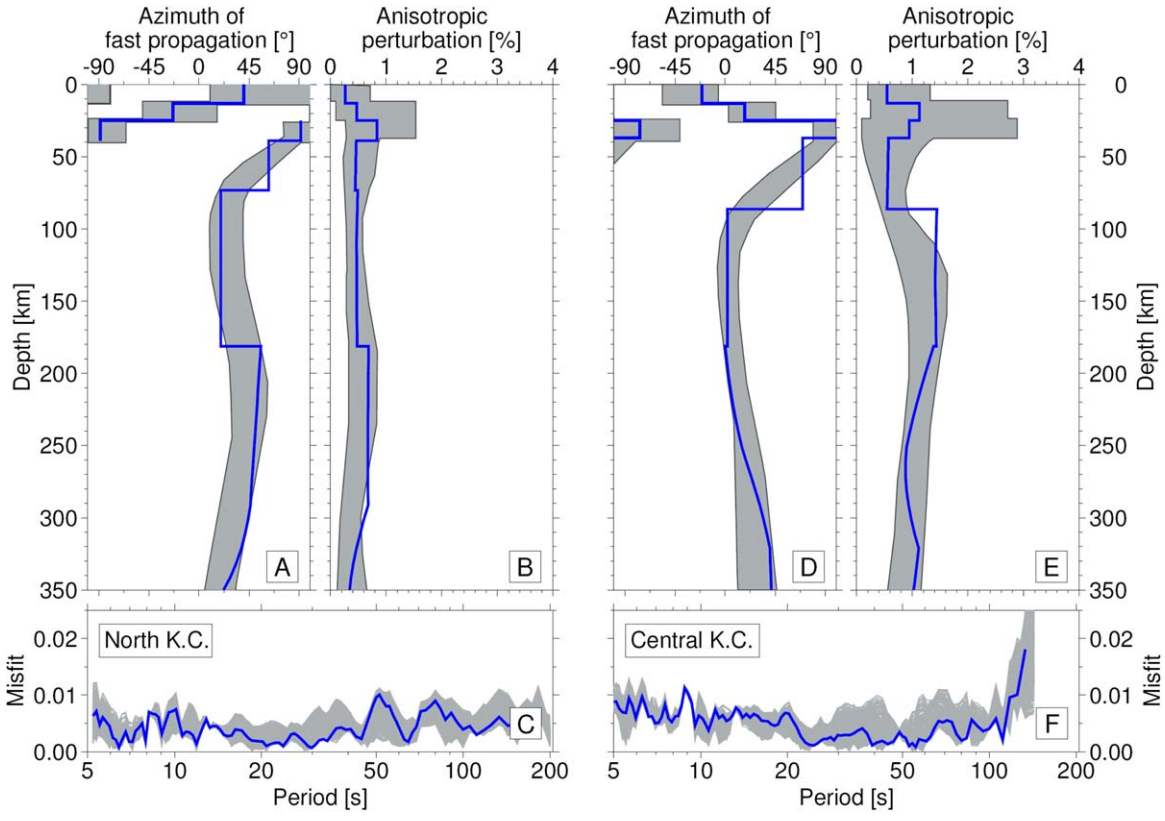

Figure 9. Azimuthal, shear-wave velocity anisotropy beneath the (a–c) northern and (d–f) central Kaapvaal Craton. The azimuth of fast propagation (a and d) is relative to North (0°), and the amplitude of anisotropy (b and e) is relative to the isotropic-average versus gray bands (a, b, d, e) enclose models that are smooth in the upper mantle and fit the data approximately equally well. Blue lines show the models in which the upper mantle down to ~200 km was parameterized with two boxcar basis functions, with three discontinuities above, below, and between them which were allowed to move up and down during the inversion. Misfits for all the models are shown in Figures 9c and 9f. The change in the fast-propagation azimuth around 80–90 km depth is present in all models that fit the data and is a robust result of the inversions.

splitting [*Vinnik et al*., 2012]. Considering the distribution of SRF piercing points (Figure 4), the results of our models are directly applicable across much of the Kaapvaal Craton, where surface-wave inversion shows S-wave fast-propagation directions around 60° azimuth (Figure 9).

[30] More generally, our results show that a discontinuity (or a steep gradient) in azimuthal anisotropy can account for the mid-lithospheric discontinuities displayed by recent SRF studies. Our choice of an isotropic medium below the discontinuity at 85–90 km is appropriate for the purposes of a general test; the models are simple and yield approximately average conversion amplitudes, smaller than if the layer below the discontinuity was anisotropic and with fast-propagation azimuth perpendicular to that in the layer above, but larger than if the two anisotropic layers had nearly parallel fast-propagation azimuths. We interpret LVZ1 at 85 km depth as a MLD caused by changes in seismic anisotropy, which may be related to the creation of the Kalahari Craton in Archean times (Figure 11). The depth of this discontinuity is in good agreement with that of the 8° discontinuity, which was earlier seen in dense long-range seismic profiles and suggested as a global characteristic of the cratonic lithosphere [*Thybo and Perchuc*, 1997; *Thybo*, 2006].

[31] To better characterize the other observed negative velocity contrasts, we first compare our results with those derived from geochemical observations. Based on the compositional and thermal state of the lithospheric mantle beneath the Kalahari Craton as inferred from xenoliths and xenocrysts [e.g., *Griffin et al*., 2003a, 2003b; *Begg et al*., 2009], the original Archean lithosphere of the Kalahari Craton has undergone several magmatic events, which changed the composition and

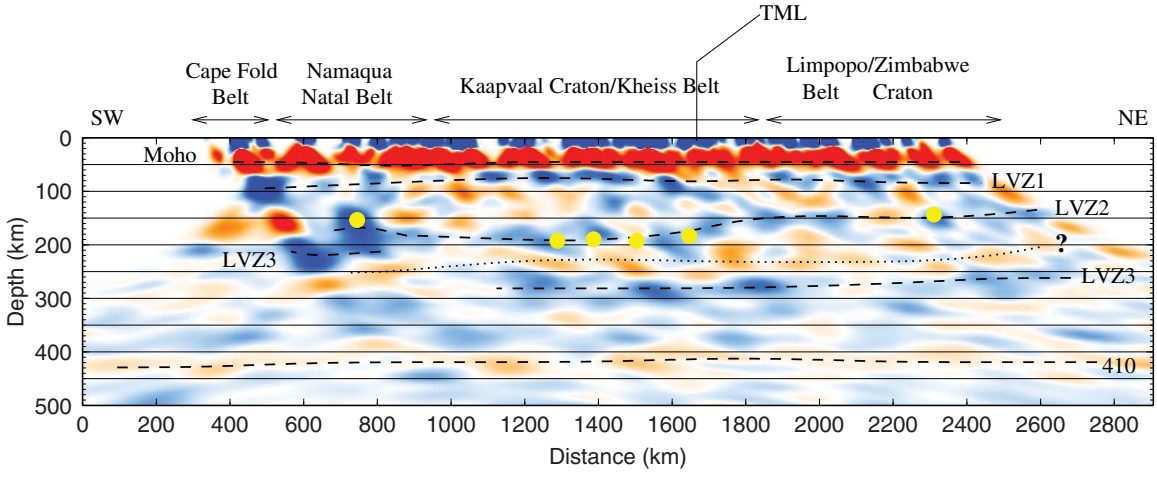

Figure 10. Migrated SRFs along the SW-NE profile shown in Figure 4. Positive (negative) phases are shown in red (blue). Yellow dots represent the depth of the boundary between depleted and fertile lithospheric mantle inferred from chemical tomography [*Begg et al*., 2009]. Seismic discontinuities are marked with black dashed lines. In addition to the Moho boundary and the 410 km discontinuity, three LVZs are evident in the migrated SRFs. LVZ1 is observed at depths of about 80–90 km beneath the whole profile. The depth of LVZ2 (150–200 km) is well correlated with that obtained from kimberlite xenoliths (yellow dots) in southern Africa. It is located at shallower depths beneath the northern part of the profile (∼150 km) compared to the central and southern parts of the profile (∼200 km). Beneath the Namaqua-Natal belt, it seems to continue at shallower depths (∼150 km). LVZ3 appears as a strong discontinuity at 260–280 km depth beneath the whole profile, up to the Namaqua-Natal belt, where it may be located at 200–220 km depth (short black dashed line at 500–800 km distance). There is also evidence for a significant positive discontinuity at depths of about 230–240 km (black dotted line).

thus the seismic velocity of the mantle (Figure 4). Chemical tomography sections from the Kalahari Craton clearly exhibit a level of metasomatic refertilization of the originally highly depleted mantle, producing a significant change in the seismic velocity at depths of 150–220 km [*Begg et al*., 2009]. The widespread occurrence of kimberlite nodules within the Kalahari Craton enabled us to directly compare the depths of our LVZs with those from kimberlite xenoliths (Figure 10). Our comparison indicates a significant correlation between the two data sets. Kimberlite xenoliths found in the central and southern Kalahari Craton (e.g. Premier, Kroonstadt, Schweitzer Renecke, South Botswana) [see *Griffin et al*., 2003a; *Begg et al*., 2009], which may have been altered by ancient magmatic events (e.g., Bushveld (2.05 Ga), Ventersdrop (2.7Ga)), sampled the original depleted lithosphere down to depths of 180–200 km. This depth is consistent with that of our LVZ2 beneath the Kaapvaal Craton and the Kheiss belt. At the same time, the highly depleted lithosphere marked by xenoliths from the northern half of the area (e.g., Zambezi Rift), which has been mainly disturbed by recent magmatic events (e.g., Karoo flood-basalt, 183 Ma) was shown at depths of 140–150 km. This depth corresponds to that of our LVZ2 beneath the Zimbabwe Craton, the Limpopo belt, and the northernmost Kaapvaal Craton. Beneath the Namaqua-Natal belt, LVZ2 may shallow to a depth of about 170 km, which is in reasonable agreement with the depth (150 km) inferred from Namaqua kimberlite xenoliths, when considering the likely error in depth estimation of about 10 km [see *Griffin et al*., 2003a; *Begg et al*., 2009]. However, the presence of another sharp negative discontinuity at 200–220 km is also evident in the SRF image beneath this younger Proterozoic belt (Figure 10).

[32] Given the spatial distribution of major magmatic events that altered the mantle lithosphere of the Kalahari Craton (Figure 4), our results may imply that the Mesozoic Karoo dike swarm (183 Ma), which cuts across the Limpopo terrane and the Zimbabwe Craton, has affected the mantle lithosphere of the northern part of the region in the same way that the formation of the Bushveld complex (2.05 Ga) and Ventersdrop (2.7 Ga) influenced the mantle lithosphere of the central and southern Kaapvaal, but probably more intensely. Moreover, the Namaqua-Natal belt may represent a Proterozoic belt with a thinner and more fertile

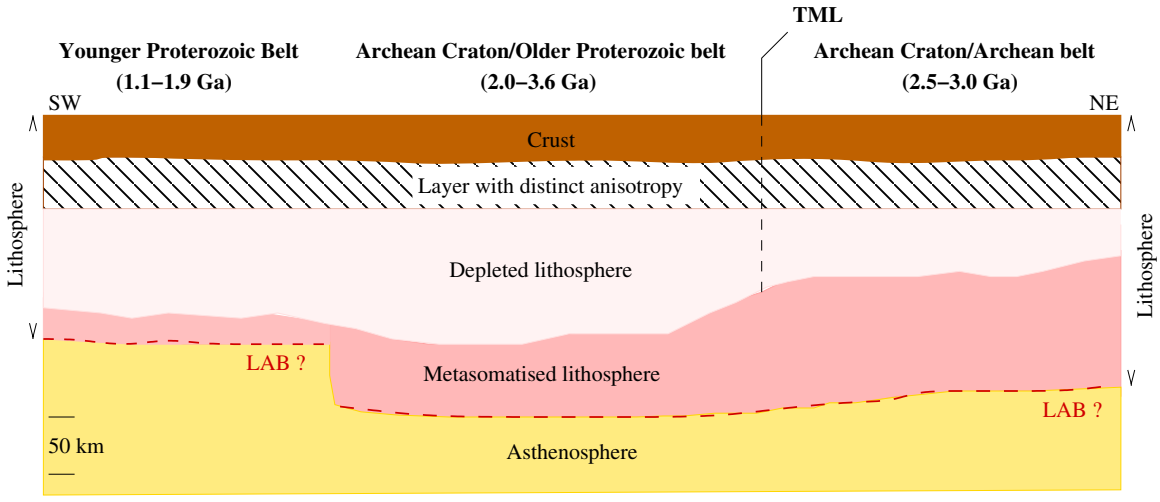

Figure 11. Sketch of our suggested layered structure of the mantle lithosphere beneath the Kalahari Craton. The mantle lithosphere consists of three layers. A layer with distinct anisotropy (i.e., anisotropy that is different from that in the layer below), with a thickness of about 50 km, is apparent beneath the whole Kalahari Craton and builds the first layer of the stratified lithosphere. The bottom of the second layer coincides with significant compositional changes. The thickness of this layer is different beneath terranes with different ages. The TML seems to act as a boundary separating the modified lithosphere (mainly by recent magmatism) of Archean craton/belt (2.5–3 Ga) in the NE from the perturbed Archean terrane and Proterozoic belt (2.0–3.6 Ga, mainly by ancient magmatism). The LAB (dark red dashed line) seems to be relatively strong and may lie at depths of about 260–280 km beneath the Archean domains and older Proterozoic belt. It appears to be much shallower (~200 km) beneath the younger Proterozoic belt (1.1–1.9 Ga).

mantle lithosphere. Unfortunately, insufficient resolution at the margin of our coverage did not allow us to locate this boundary beneath the Mozambique and Cape Fold belts.

[33] The strong correlation between mantle composition and the lateral variations in depth of LVZ2 lead us to interpret this boundary as a compositional boundary resulting from the magmatic events that perturbed the original Archean lithosphere of the Kalahari Craton (Figure 10). However, it is not clear whether this boundary constrains the maximum thickness of the lithospheric mantle or not. Based on our findings and those obtained from chemical tomography, we characterize the Thabazimbi-Murchison Lineament as a translithospheric boundary (Figure 4), which appears to form and influence the boundary between the Archean terrane of the Kaapvaal and the southern margin of the high grade terrane of the Limpopo belt and separates these two distinct lithospheric blocks from each other (Figure 10).

[34] Recently, *Savage and Silver* [2008] attributed a discontinuity at 150 km depth beneath the Zimbabwe Craton and the Limpopo belt to the metasomatising influence of melt infiltration, mainly associated with the Karoo magmatism. Their findings were, however, limited in the northern part of our study area. In addition, *Wittlinger and Farra* [2007] observed significant disagreement between the depth of the highly depleted mantle inferred from geochemical data and that deduced from their SRF results near Kroonstadt, located in the central part of our profile. No negative velocity contrast has been detected at this inferred depth (200 km) in their SRF data, where we imaged LVZ2 at about 200 km depth. A lithospheric-mantle model [*Muller et al*., 2013], which simultaneously satisfied all geophysical and geochemical observations beneath the Kaapvaal Craton (magnetotelluric, SRF, heat flow, xenolith, surface elevation, and surface-wave dispersion) shows that a three-layered geochemical model, with lithospheric thickness larger than 230 km, is required to match all geophysical and xenolith constraints. This depth is considerably larger than that suggested by recent SRF studies (140–160 km), but is more consistent with our LVZ3.

[35] We are able to image LVZ3 as a relatively constant boundary throughout the Archean domains up to the Namaqua-Natal belt (Figure 10). LVZ3 seems to be flat and lies at 280 km

depth beneath the Kaapvaal Craton and the Kheiss belt, and it gently shallows (to 260 km depth) northward beneath the Zimbabwe Craton and the Limpopo belt. Furthermore, it appears to be a stronger velocity contrast (~4.7%) beneath the Kaapvaal Craton and its passive margin compared to the Zimbabwe Craton and the Limpopo belt (~3.6%). The depth of this boundary is a little shallower than that inferred for the LAB in P receiver function analysis (~300 km, Table 1).

[36] Similar results to those presented here were also obtained for the North American Craton and Hudson Bay basin by *Yuan and Romanowicz* [2010] and *Darbyshire et al*. [2013], respectively. Vertical stratification of the thick cratonic lithosphere was resolved by seismic velocities and changes in azimuthal anisotropy. The upper lithospheric layer was interpreted as the highly depleted layer, which was suggested by kimberlite xenoliths and was also inferred by SRF analysis. Whereas the more fertile lower lithosphere was recognized to be limited by a thermal boundary that may have formed in post-Archean times, this boundary was not detected by SRFs in these studies. Our interpretation for LVZ2 as a compositional boundary is consistent with that suggested beneath the North American Craton. We find no evidence for an anisotropy-related origin either for this discontinuity or for LVZ3 (Figure 6). Moreover, the clear appearance of both boundaries (LVZ2, LVZ3) in the SRF data excludes a purely thermal origin for these discontinuities.

[37] Modeling based on the mean composition and thermal states of Archean lithosphere indicates that the buoyant Archean mantle lithosphere would tend to survive during rifting and collisional events but would be cumulatively transformed to more fertile composition with lower velocities [e.g., *Griffin et al*., 1999; *Poudjom Djomani et al*., 2001]. Therefore, there is no compelling evidence that the melt-metasomatized zone apparently identified by xenoliths is underlain by convecting mantle and represents the base of the lithosphere. An alternative interpretation would be that the passage of large volumes of magma through the lithosphere due to subsequent magmatic events gives rise to a compositional boundary within the lithosphere, indicating a level where mantle-derived melt has accumulated and metasomatized. In this case, LVZ2 may likely indicate a MLD marking a notable compositional change (Figure 11). This interpretation can also account for LVZ3, which is a stronger boundary than LVZ2, and is most clearly seen beneath the Archean domains. Disappearance of LVZ3 beneath the Namaqua-Natal belt (youngest mobile belt ~1.2 Ga), which might have been generated in Proterozoic time [*Griffin et al*., 2003a], and the strong appearance of LVZ3 beneath the Archean Kaapvaal Craton and its passive margin (~2.7–3.6 Ga) may imply the presence of a thick lithospheric root (260–280 km) beneath the Kalahari Craton. However, this thick root is limited to the Archean terranes and older Proterozoic belts (~2.0–3.6 Ga; Figure 11). The younger Namaqua-Natal belt that has been later accreted to the Kaapvaal Craton from the south [*Griffin et al*., 2003a] may be underlain by a much shallower LAB at about 200–220 km depth (Figures 5 and 10).

[38] Our interpretation may imply a relation between the LAB depth and the age of the terrane, indicating that the LAB is shallower (200 km) beneath the younger Proterozoic mobile belt (~1.1–1.9 Ga) and deeper (260–280 km) beneath the Archean domains and older belts (~2–2.6 Ga; Figure 11). These results are in contrast with those inferred for the Laurentian mantle keel [*Darbyshire et al*., 2013], where no correlation between crustal age and lithospheric thickness was found. Furthermore, we cannot determine from our results whether the accretion of the lower metasomatised lithosphere (Figure 11) to the upper layer (depleted lithosphere) happened during the Archean times or later.

[39] Based on our analysis, the LAB (LVZ3) appears to be a prominent (3.6–4.7 %) discontinuity beneath the whole Kalahari Craton, and it is unlikely associated with a significant change in temperature or composition. Instead, another mechanism may be required, such as melting or dehydration. We suggest that the thick lithosphere of the Kalahari Craton (~260–280 km) may have resisted structural changes since its formation, probably due to the depletion of the mantle lithosphere. However, infiltration of metasomatic fluids due to major magmatic events may have gradually altered the mantle lithosphere and generated considerable changes in its composition. Finally, sharp boundaries generated by frozen-in anisotropy and significant compositional changes can result in an irregularly stratified structure, which can be identified by SRFs.

6. Conclusions

[40] To further our understanding of the formation and evolution of the mantle lithosphere beneath the Kalahari Craton, we have jointly analyzed S receiver functions and azimuthal anisotropy from surface waves. SRFs obtained from teleseismic data recorded by 97 stations clearly characterize a thick

and stratified lithosphere beneath the Kalahari Craton. In particular, the SRFs resolve three significant negative velocity contrasts at 85, 150–200, and 260–280 km depth. Moreover, a layer with distinct anisotropy in the uppermost mantle (down to around 80–90 km) is clearly detected by both the SRFs and surface wave data. Our results imply that frozen-in anisotropy as well as notable compositional variations can lead to sharp Mid-Lithospheric Discontinuities (MLD) that can be clearly observed in the SRF data. We show that a 50 km thick anisotropic layer just below the Moho boundary with 3% S wave anisotropy may be responsible for producing a MLD at 85 km depth. This feature probably corresponds to the 8° discontinuity seen in dense, long-range seismic profiles. The horizontal anisotropy in the upper lithosphere may be attributed to processes during the formation of the Kalahari Craton.

[41] We also find a notable consistency in the lateral variations of the depth of the negative discontinuity observed at 150–200 km depth in our data and the depth of the bottom of highly depleted lithospheric mantle inferred from kimberlite xenoliths. This agreement supports an interpretation of this MLD as a compositional boundary associated with magmatic events within the Kalahari Craton. This boundary is seen at about 150 km depth beneath the northern part of the Kalahari Craton (Zimbabwe Craton, Limpopo belt), and it abruptly deepens to about 200 km beneath the Kaapvaal Craton and its passive margin in the south. The sudden deepening of this discontinuity occurs beneath the surficial appearance of the TML, suggesting the TML is a translithospheric boundary separating the older Archean Kaapvaal terrane from the younger Limpopo belt. Furthermore, the LAB may be identified as a strong boundary with a large velocity contrast (3.6–4.7%) at depths of about 260–280 km beneath the Archean domains and older Proterozoic mobile belt. This boundary appears to be much shallower (~200–220 km) beneath the younger Proterozoic Namaqua-Natal belt. Thus, our results rule out the thermal and compositional nature of the LAB and instead may require additional mechanisms, such as melting and dehydration, to explain its strong seismic visibility.

Acknowledgments

[42] This research has been funded by Deutsche Forschungsgemeinschaft. Seismic data were provided by IRIS, AfricaArray. We used the ray theory code [*Frederiksen and Bostock*, 2000] for numerical modeling. We wish to thank the Associate Editor and two anonymous reviewers for their helpful and constructive comments that improved the paper.

References

Abt, D. L., K. M. Fischer, S. W. French, H. A. Ford, H. Yuan, and B. Romanowicz (2010), North American lithospheric discontinuity structure imaged by Ps and Sp receiver functions, *J. Geophys. Res.*, *115*, B09301, doi:10.1029/2009JB006914.

Adam, J. M.-C., and S. Lebedev (2012), Azimuthal anisotropy beneath southern Africa from very broad-band surface-wave dispersion measurements, *Geophys. J. Int.*, *191*, 155–174, doi:10.1111/j.1365-246X.2012.05583.x.

Adam, J. M.-C. (2013), *Seismic structure and anisotropy in southern Africa's lithosphere: Constraints from broad-band surface-wave dispersion*, PhD thesis, Trinity College Dublin.

Adams, A., and A. Nyblade (2011), Shear wave velocity structure of the southern African upper mantle with implications for the uplift of southern Africa, *Geophys. J. Int.*, *186*, 808–824, doi:10.1111/j.1365-246X.2011.05072.x.

Agius, M. R., and S. Lebedev (2013), Tibetan and Indian lithospheres in the upper mantle beneath Tibet: Evidence from broadband surface-wave dispersion, *Geochem. Geophys. Geosyst.*, *14*, doi:10.1002/ggge.20274.

Armstrong, R. A. (1987), *Geochronological studies on Archaean and Proterozoic formations of the foreland of the Namaqua front and possible correlates on the Kaapvaal Craton*, PhD thesis, 274 pp., Witwatersrand Univ., Johannesburg.

Artemieva, I. M. (2009), The continental lithosphere: Reconciling thermal, seismic, and petrologic data, *Lithos*, *109*, 23–46.

Artemieva, I., and W. D. Mooney (2001), Thermal thickness and evolution of Precambrian lithosphere: A global study, *J. Geophys. Res.*, *106*(B8), 16,387–16,414.

Ashwal, L., and K. Burke (1989), African lithospheric structure, volcanism, and topography, *Earth planet. Sci. Lett.*, *96*, 8–14.

Barton, Jr., J. M., L. Holzer, and B. Kamber (1994), Discrete metamorphic events in the Limpopo belt, southern Africa: Implications for application of P– T paths in complex metamorphic terrains, *Geology*, *22*, 1035–1038.

Bartzsch, S., S. Lebedev, and T. Meier (2011), Resolving the lithosphere-asthenosphere boundary with seismic Rayleigh waves, *Geophys. J. Int.*, *186*, 1152–1164, doi:10.1111/j.1365-246X.2011.05096.x.

Becker, T. W., S. Chevrot, V. Schulte-Pelkum, and D. K. Blackman (2006), Statistical properties of seismic anisotropy predicted by upper mantle geodynamic models, *J. Geophys. Res.*, *111*, B08309, doi:10.1029/2005JB004095.

Begg, G. C., et al. (2009), The lithospheric architecture of Africa: Seismic tomography, mantle petrology, and tectonic evolution, *Geosphere*, *5*, 23–50, doi:10.1130/GES00179.1.

Bostock, M. G. (1998), Mantle stratigraphy and evolution of the Slave province, *J. Geophys. Res.*, *103*(B9), 21,183–21,200.

Boyd, F., and S. Mertzman (1987), Composition and structure of the Kaapvaal lithosphere, southern Africa, in Magmatic Processes, Physicochemical Principles, edited by B. Mysen, pp. 13–24, Geochem. Soc., Univ. of Pennsylvania, University Park, Pa.

Boyd, F., D. Pearson, and S. Mertzman (1999), Spinel-facies peridotites from the Kaapvaal Root, in Proceedings of the 7th International Kimberlite Conference, *The J.B. Dawson*

Volume, pp. 40–49, edited by J. Gurney, Red Roof Design, Cape Town, S. Afr.

Cammarano, F., and B. Romanowicz (2007), Insights into the nature of the transition zone from physically constrained inversion of long-period seismic data, *Proc. Natl. Acad. Sci., U. S. A.*, *104*, 9139–9144.

Carlson, R. W., T. L. Grove, M. J. de Wit, and J. J. Gurney (1996), Anatomy of an Archean craton: A program for interdisciplinary studies of the Kaapvaal Craton, *southern Africa, Eos Trans. AGU*, *77*, 273–277.

Chen, L. (2009), Lithospheric structure variations between the eastern and central North China Craton from S- and P-receiver function migration, *Phys. Earth Planet. Inter.*, *173*, 216–227.

Chevrot, S., and L. Zhao (2007), Multiscale finite-frequency Rayleigh wave tomography of the Kaapvaal Craton, *Geophys. J. Int.*, *169*, 201–215.

Cornell, D. H., R. A. Armstrong, and F. Walraven (1998), Geochronology of the Proterozoic Hartley Basalt Formation, South Africa: Constraints on the Kheis tectogenesis and the Kaapvaal Craton's earliest Wilson cycle, *J. Afr. Earth Sci.*, *26*(1), 5–27.

Darbyshire, F., D. W. Eaton, and I. D. Bastow (2013), Seismic imaging of the lithosphere beneath Hudson Bay: Episodic growth of the Laurentian mantle keel, *Earth Planet. Sci. Lett.*, *373*, 179–193, doi:10.1016/j.epsl.2013.05.002.

de Wit, M. J., Ch. Roering, R. G. Hart, R. A. Armstrong, C. E. J. de Ronde, R. W. E. Green, M. Tredoux, E. Peberdy, and R. A. Hart (1992), Formation of an Archean continent, *Nature*, *357*, 553–562.

Durrheim, R. J., W. H. Barker, and R. W. E. Green (1992), Seismic studies in the Limpopo Belt, *Precambrian Res.*, *55*, 187–200.

Eaton, D. W., F. Darbyshire, R. L. Evans, H. Grutter, A. G. Jones, and X. Yuan (2009), The elusive lithosphere-asthenosphere boundary (LAB) beneath cratons, *Lithos*, *109*, 1–22.

Farra, V., and L. Vinnik (2000), Upper mantle stratification by P and S receiver functions, *Geophys. J. Int.*, *141*, 699–712, doi:10.1046/j.1365-246x.2000.00118.x.

Fischer, K. M., H. A. Ford, D. L. Abt, and C. A. Rychert (2010), The lithosphere-asthenosphere boundary, *Annu. Rev. Earth Planet. Sci.*, *38*, 551–575, doi:10.1146/annurev-earth-040809–152438.

Fishwick, S. (2010), Surface wave tomography: Imaging of the lithosphere-asthenosphere boundary beneath central and south Africa, *Lithos*, *120*, 63–73, doi:10.1016/j.lithos.2010.05.011.

Ford, H. A., K. M. Fischer, D. L. Abt, C. A. Rychert, and I. T. Elkins-Tanton (2010), The lithosphere-asthenosphere boundary and cratonic lithospheric layering beneath Australia from Sp wave imaging, *Earth Planet. Sci. Lett.*, *300*, 299–310, doi:10.1016/j.epsl.2010.10.007.

Fouch, M. J., D. E. James, J. C. van der Car, S. van der Lee, and The Kaapvaal Seismic Group (2004), Mantle seismic structure beneath the Kaapvaal and Zimbabwe cratons, *South Afr. J. Geol.*, *107*, 33–44.

Frederiksen, A. W., and M. G. Bostock (2000), Modelling teleseismic waves in dipping anisotropic structures, *Geophys. J. Int.*, *141*, 401–412.

Frei, R., T. G. Blenkinsop, and R. Shonberg (1999), Geochronology of the late Archean Razi and Chilimanzi suites of granites in Zimbabwe: Implications for the late Archean tectonics of the Limpopo belt and Zimbabwe craton, *S. Afr. J. Geol.*, *102*, 55–63.

Gaherty, J. B. (2004), A surface wave analysis of seismic anisotropy beneath eastern North America, *Geophys. J. Int.*, *158*, 1053–1066.

Gaherty, J. B., and T. H. Jordan (1995), Lehmann discontinuity as the base of an anisotropic layer beneath continents, *Science*, *268*, 1468–1471, doi:10.1126/science.268.5216.1468.

Geissler, W. H., F. Sodoudi, and R. Kind (2010), Thickness of the central and eastern European lithosphere as seen by S receiver functions, *Geophys. J. Int.*, *181*(2), 604–634, doi:10.1111/j.1365-246X.2010.0.

Good, N., and M. J. de Wit (1997), The Thabazimbi-Murchison Lineament of the Kaapvaal Craton, South Africa: 2700 Ma of episodic deformation, *J. Geol. Soc.*, *154*, 93–97, doi:10.1144/gsjgs.154.1.0093.

Goodwin, A. M. (1996), *Precambrian Geology*, 327 pp., Academic, London.

Grand, S. P. (2002), Mantle shear-wave tomography and the fate of subducted slabs, *Philos. Trans. R. Soc. A*, *360*, 2475–2491, doi:10.1098/rsta.2002.1077.

Grand, S. P., and D. V. Helmberger (1984), Upper mantle shear structure of North America, *Geophys. J. R. Astron. Soc.*, *76*, 399–438.

Griffin, W. L., S. Y. O'Reilly, and C. G. Ryan (1999), The composition and origin of subcontinental lithospheric mantle, in Mantle Petrology: Field Ob-servations and High-Pressure Experimentation: A Tribute to Francis R. (Joe) Boyd, edited by Y. Fei, C. M. Bertka, and B. O. Mysen, Geochem. Soc. Spec. Publ., vol. *6*, pp. 13–45, The Geochemical Society, Houston, Tex.

Griffin, W. L., S. Y. O'Reilly, L. M. Natapov, and C. G. Ryan (2003a), The evolution of lithospheric mantle beneath the Kalahari Craton and its margins, *Lithos*, *71*, 215–241, doi:10.1016/j.lithos.2003.07.006.

Griffin, W. L., S. Y. O'Reilly, N. Abe, S. Aulbach, R. M. Davies, N. J. Pearson, B. J. Doyle, and K. Kivi (2003b), The origin and evolution of Archean lithospheric mantle, *Precambrian Res.*, *127*, 19–41, doi:10.1016/S0301–9268(03)00180-3.

Gung, Y. C., M. Panning, and B. Romanowicz (2003), Global anisotropy and the thickness of continents, *Nature*, *422*, 707–711.

Gurney, J., and B. Harte (1980), Chemical variations in upper mantle nodules from southern African kimberlites, *Philos. Trans. R. Soc. A*, *297*, 273–293.

Hansen, S. E., A. A. Nyblade, J. Julia, P. H. G. M. Dirks, and R. J. Durrheim (2009), Upper-mantle low-velocity zone structure beneath the Kaapvaal craton from S-wave receiver functions, *Geophys. J. Int.*, *178*, 1021–1027.

Heit, B., F. Sodoudi, X. Yuan, M. Bianchi, and R. Kind (2007), An S receiver function analysis of the lithospheric structure in South America, *Geophys. Res. Lett.*, *34*, L14397, doi:10.1029/2007GL030317.

Hirth, G., R. L. Evans, and A. D. Chave (2000), Comparison of continental and oceanic mantle electrical conductivity: Is the Archean lithosphere dry?, *Geochem. Geophys. Geosyst.*, *1*(12), 1030, doi:10.1029/2000GC000048.

James, D. E., M. J. Fouch, J. C. van de Car, S. van der Lee, and the Kaapvaal group (2001), Tectospheric structure beneath southern Africa, *Geophys. Res. Lett.*, *13*, 2485–2488.

James, D. E., F. R. Boyd, D. Schutt, D. R. Bell, and R. W. Carlson (2004), Xenolith constraints on seismic velocities in the upper mantle beneath southern Africa, *Geochem. Geophys. Geosyst.*, *5*, Q01002, doi:10.1029/2003GC000551.

Jaupart, C., J. C. Mareschal, L. Guillou-Frottier, and A. Davaille (1998), Heat flow and thickness of the lithosphere in the Canadian Shield, *J. Geophys. Res.*, *103*, 15,269–15,286.

Jones, A. G., R. L. Evans, and D. W. Eaton (2009), Velocity-conductivity relationships for mantle mineral assemblages in Archean cratonic lithosphere based on a review of laboratory data and Hashin-Shtrikman extermal bounds, *Lithos*, *109*, 131–143, doi:10.1016/j.lithos.2008.10.014.

Jones, A. G., J. Plomerova, T. Korja, and F. Sodoudi (2010), Europe from the bottom up: A statistical examination of the central and northern European lithosphere-asthenosphere boundary from comparing seismological and electromagnetic observations, *Lithos*, *120*, 14–29.

Jordan, T. (1975), The continental tectosphere, *Rev. Geophys.*, *13*, 1–12.

Karato, S. (2010), Rheology of the deep upper mantle and its implications for the preservation of the continental root: A review, *Tectonophysics*, *481*, 82–98.

Karato, S. (2012), On the origin of the asthenosphere, *Earth Planet. Sci. Lett.*, *321–322*, 95–103.

Kennett, B. L. N., and E. R. Engdahl (1991), Traveltimes for global earthquake location and phase identification, *Geophys. J. Int.*, *105*, 429–465, doi:10.1111/j.1365-246X.1991.tb06724.x.

Kind, R., et al. (2013), Scandinavia: A former Tibet?, *Geochem. Geophys. Geosyst.*, *14*, doi:10.1002/ggge.20251.

Kind, R., X. Yuan, and P. Kumar (2012), Seismic receiver functions and the lithosphere-asthenosphere boundary, *Tectonophysics*, *536–537*, 25–43.

Kumar, P., et al. (2007), The rapid drift of the Indian tectonic plate, *Nature*, *449*, 894–897.

Kumar, P., R. Kind, X. Yuan, and J. Mechie (2012), USArray receiver function images of the lithosphere-asthenosphere boundary, *Seismol. Res. Lett.*, *83*, 486–491.

Kumar, P., X. Yuan, R. Kind, and J. Ni (2006), Imaging the colliding Indian and Asian continental lithospheric plates beneath Tibet, *J. Geophys. Res.*, *111*, B06308, doi:10.1029/2005JB003930.

Kustowski, B., G. Ekstrom, and A. M. Dziewonski (2008), Anisotropic shear-wave velocity structure of the Earth's mantle: A global model, *J. Geophys. Res.*, *113*, B06306, doi:10.1029/2007JB005169.

Li, A., and K. Burke (2006), Upper mantle structure of southern Africa from Rayleigh wave tomography, *J. Geophys. Res.*, *111*, doi:10.1029/2006JB004321.

Lebedev, S., and R. D. van der Hilst (2008), Global upper-mantle tomography with the automated multimode inversion of surface and S-wave forms, *Geophys. J. Int.*, *173*, 505–518.

Lebedev, S., J. Boonen, and J. Trampert (2009), Seismic structure of Precambrian lithosphere: New constraints from broad-band surface-wave dispersion, *Lithos*, *109*, 96–111.

Levin, V., and J. Park (1997), P-SH conversions in a flat-layered medium with anisotropy of arbitrary orientation, *Geophys. J. Int.*, *131*, 253–266.

Levin, V., and J. Park (1998), P-SH conversions in layered media with hexagonally symmetric anisotropy: a cookbook, *Pure Appl. Geophys.*, *151*, 669–697.

Long, M. D., and T. W. Becker (2010), Mantle dynamics and seismic anisotropy, *Earth Planet. Sci. Lett.*, *297*, 341–354.

Matthews, P. E. (1981), Eastern or Natal sector of the Namaqua—Natal mobile belt in Southern Africa, in Precambrian of the Southern Hemisphere, edited by D. R. Hantner, pp. 705–715, Elsevier, Amsterdam.

Mierdel, K., H. Keppler, J. R. Smyth, and F. Langenhorst (2007), Water solubility in aluminous orthopyroxene and the origin of the Earth's asthenosphere, *Science*, *315*, 364–368.

Miller, M. S., and D. W. Eaton (2010), Formation of cratonic mantle keels by arc accretion: Evidence from S receiver functions, *Geophys. Res. Lett.*, *37*, L18305, doi:10.1029/2010GL044366.

Muller, M., J. Fullea, A. G. Jones, J. Adam, S. Lebedev, and N. P. Agostinetti (2013), Lithospheric-mantle structure of the Kaapvaal Craton, South Africa, derived from thermodynamically self-consistent modelling of magnetotelluric, surface-wave dispersion, S-wave Receiver Function, heat-flow, elevation and xenolith observations, *Geophys. Res. Abst.*, *15*, EGU2013–12903, EGU General Assembly 2013.

Plomerova, J., and V. Babuska (2010), Long memory of mantle lithosphere fabric-European LAB constrained by seismic anisotropy, *Lithos*, *120*, 131–143, doi:10.1016/j.lithos.2010.01.008.

Poudjom Djomani, Y. H., S. Y. O'Reilly, W. L. Griffin, and P. Morgan (2001), The density structure of subcontinental lithosphere: Constraints on delamination models, *Earth Planet. Sci. Lett.*, *184*, 605–621, doi:10.1016/S0012–821X(00)00362-9.

Priestley, K., and F. Tilmann (2009), Relationship between the upper mantle high velocity seismic lid and the continental lithosphere, *Lithos*, *109*, 112–124.

Priestley, K., D. McKenzie, and E. Debayle (2006), The state of the upper mantle beneath southern Africa, *Tectonophysics*, *416*, 101–112.

Priestley, K., D. McKenzie, E. Debayle, and S. Pilidou (2008), The African upper mantle and its relationship to tectonics and surface geology, *Geophys. J. Int.*, *175*, 1108–1126, doi:10.1111/j.1365-246X.2008.03951.x.

Romanowicz, B. (2009), The thickness of tectonic plates, *Science*, *324*, 474–476.

Rudnick, R., W. McDonough, and R. O'Connell (1998), Thermal structure, thickness and composition of continental lithosphere, *Chem. Geol.*, *145*, 395–411.

Rychert, C. A., and P. M. Shearer (2009), A global view of the lithosphere-asthenosphere boundary, *Science*, *324*(5926), 495–498.

Rychert, C. A., P. M. Shearer, and K. M. Fischer (2010), Scattered wave imaging of the lithosphere–asthenosphere boundary, *Lithos*, *120*, 173–185.

Savage, M. K. (1998), Lower crustal anisotropy or dipping boundaries? Effects on receiver functions, *J. Geophys. Res.*, *103*, 15,069–15,087.

Savage, B., and P. G. Silver (2008), Evidence for a compositional boundary within the lithospheric mantle beneath the Kalahari Craton from S receiver functions, *Earth Planet. Sci. Lett.*, *272*, 600–609.

Schaeffer, A. J., and S. Lebedev (2013), Global shear speed structure of the upper mantle and transition zone, *Geophys. J. Int.*, *194*(1), 417–449.

Sebai, A., E. Stutzmann, J. P. Montagner, D. Sicilia, and E. Beucler (2006), Anisotropic structure of the African upper mantle from Rayleigh and Love wave tomography, *Phys. Earth Planet. Inter.*, *155*, 48–62, doi:10.1016/j.pepi.2005.09.009.

Shapiro, S. S., B. H. Hager, and T. H. Jordan (1999), Stability and dynamics of the continental tectosphere, *Lithos*, *48*, 115–133.

Silver, P. G. (1996), Seismic anisotropy beneath the continents: Probing the depths of geology, *Annu. Rev. Earth Planet. Sci.*, *24*, 385–432.

Silver, P. G., S. S. Gao, K. H. Liu, and the Kaapvaal group (2001), Mantle deformation beneath southern Africa, *Geophys. Res. Lett.*, *28*, 2493–2496.

Silver, P. G., M. J. Fouch, S. S Gao, M. Schmitz, and the Kaapvaal Seismic Group (2004), Seismic anisotropy, mantle fabric and the magmatic evolution of Precambrian southern Africa, *South Afr. J. Geol.*, *107*, 45–48.

Sodoudi, F., X. Yuan, Q. Liu, R. Kind, and J. Chen (2006a), Lithospheric thickness beneath the Dabie Shan, central eastern China from S receiver functions, *Geophys. J. Int.*, *166*(3), 1363–1367.

Sodoudi, F., R. Kind, D. Hatzfeld, K. Priestley, W. Hanka, K. Wylegalla, G. Stavrakakis, A. Vafidis, H. P. Harjes, and M. Bohnhoff (2006b), Lithospheric structure of the Aegean obtained from P and S receiver functions, *J. Geophys. Res.*, *111*, B12307, doi:10.1029/2005JB003932.

Sodoudi, F., X. Yuan, R. Kind, B. Heit, and A. Sadidkhouy (2009), Evidence for a missing crustal root and a thin lithosphere beneath the Central Alborz by receiver function studies, *Geophys. J. Int.*, *177*(2), 733–742.

Sodoudi, F., X. Yuan, G. Asch, and R. Kind (2011), High-resolution image of the geometry and thickness of the subducting Nazca lithosphere beneath northern Chile, *J. Geophys. Res.*, *116*, B04302, doi:10.1029/2010JB007829.

Thybo, H. (2006), The heterogeneous upper mantle low velocity zone, *Tectonophysics*, *416*, 53–79.

Thybo, H., and E. Perchuc (1997), The seismic 8° discontinuity and partial melting in continental mantle, *Science*, *275*, 1626–1629.

Vinnik, L. P., R. W. E. Green, and L. O. Nicolaysen (1995), Recent deformations of the deep continental root beneath southern Africa, *Nature*, *375*, 50–52.

Vinnik, L. P., R. W. E. Green, L. O. Nicolaysen, G. L. Kosarev, and N. V. Petersen (1996), Deep seismic structure of the Kaapvaal Craton, *Tectonophysics*, *262*, 67–75.

Vinnik, L., S. Oreshin, G. Kosarev, S. Kiselev, and L. Makeyeva (2009), Mantle anomalies beneath southern Africa: Evidence from seismic S and P receiver functions, *Geophys. J. Int.*, *179*, 279–298.

Vinnik, L., S. Kiselev, M. Weber, S. Oreshin, and L. Makeyeva (2012), Frozen and active seismic anisotropy beneath southern Africa, *Geophys. Res. Lett.*, *39*, L08301, doi:10.1029/2012GL051326.

Wittlinger, G., and V. Farra (2007), Converted waves reveal a thick and layered tectosphere beneath the Kalahari supercraton, *Earth Planet. Sci. Lett.*, *254*, 404–415.

Wölbern, I., G. Rümpker, K. Link, and F. Sodoudi (2012), Melt infiltration of the lower lithosphere beneath the Tanzania Craton and the Albertine rift inferred from S receiver functions, *Geochem. Geophys. Geosyst.*, *13*, Q0AK08, doi:10.1029/2012GC004167.

Yuan, H., and B. Romanowicz (2010), Lithospheric layering in the North American Craton, *Nature*, *466*, 1063–1069.

Zhao, M., C. Langston, A. Nyblade, and T. Owens (1999), Upper mantle velocity structure beneath southern Africa from modeling regional seismic data, *J. Geophys. Res.*, *104*(B3), 24,783–24,794.